Proceedings World Geothermal Congress 2015
Melbourne, Australia, 19-25 April 2015

Development of a Numerical Tool for EGS-Layout Calculations Based on 3D XFEM Fracture Propagation Simulations and Laboratory Experiments on Large Rock Samples

Willbrand K.[(1)], Siebert P.[(2)], Weber N.[(3)], Fries T.P.[(4)], Feinendegen M.[(2)], Ziegler M.[(2)], Clauser C.[(1)]

[(1)]Institute for Applied Geophysics and Geothermal Energy, E.ON ERC, RWTH Aachen University, Aachen, Germany

[(2)]Institute for Geotechnical Engineering, RWTH Aachen University, Aachen, Germany

[(3)]Chair for Computational Analysis of Technical Systems, RWTH Aachen University, Aachen, Germany

[(4)]Institute of Structural Analysis, Graz University of Technology, Graz, Austria

karen.willbrand@eonerc.rwth-aachen.de

Keywords: fluid induced fracture propagation, numerical simulation, hydraulic fracturing experiments, XFEM, enhanced geothermal systems, assessment, true triaxial testing facility, acoustic emission monitoring.

ABSTRACT

In view of engineering a heat exchanger at depth, we study the creation and optimization of fractures in basement rocks. To this end we developed a 3D fracture propagation code and verified it against laboratory hydraulic fracture experiments. Ultimately, the fracture propagation code will be coupled to an existing reservoir simulator for heat and mass transfer. It handles discontinuities, i.e. discrete fractures, by the particularly suited Extended Finite Element Method. A true-triaxial press allows verification of the code. Experiments comprise fluid-induced fracturing of rocks of a dimension of 300 × 300 × 450 mm³ under horizontal and vertical confining pressures up to 15 MPa and 30 MPa, respectively. Thirty-two ultrasonic sensors placed around the rock sample allow monitoring fracture propagation by recording and localizing the associated acoustic events during fracture propagation. The experiments help testing and improving the fracture propagation code. The ultimate goal is the development of a numerical design and layout tool for engineered geothermal systems.

1. INTRODUCTION

Conversion of deep geothermal energy into electricity bears great potential also in regions lacking natural permeability. But engineering of a heat exchanger in deep and dense formations has not yet matured into a readily deployable and economical technology [Gerard et al. 2006, Brown et al. 2012]. One way to improve the controlled siting and creation of a fracture system is to develop a numerical layout tool for simulating, evaluating and optimizing different fracture scenarios according to their long-term energetic use constrained, on the one hand, by geologic information and uncertainty and on the other hand by technological and economic viability. Here, we report the development and verification of a 3D fracture propagation code to be coupled, in the future, to an extensively tested and continuously enhanced reservoir heat and mass transport code [Clauser 2003, Rath et al. 2006]. It will be verified in a first stage against laboratory experiments and in a future stage against field experiments involving shallow boreholes (~ 100 m depth) in a crystalline rock.

We built a true-triaxial press for testing low permeability rock samples of dimension 300 x 300 x 450 mm³ in order to verify the code with laboratory-scale experiments. In section two we present its construction, abilities, and limits and the status of the ongoing verification experiments. The third section explains the numerical approach, the underlying physical model, the governing equations and their numerical realization. In the last section we summarize and provide an outlook.

2. FLUID INDUCED FRACTURE EXPERIMENTS

Our new test facility enables performing hydraulic fracturing tests on dense rock samples under confining pressure in the laboratory (Figure 1). It comprises three parts: the loading apparatus, the injection system, and the acoustic emission recording system.

2.1 True-triaxial test facility

The loading apparatus is set up for each new test, except for the bottom slab and three of four tension members which are always left in place and form the basic set up. The sample is machined into a cuboidal shape of 300 x 300 x 450 mm³ size. Further preparation involves drilling of a borehole of 20 mm diameter and cutting of a fracture nucleus in the open-hole section. After cleaning the borehole and installing the packer, the rock sample is placed into the testing frame and enclosed by loading plates. Each of these contains a number of holes through which we bring a total of 32 ultrasonic sensors in direct contact with the rock surface. Thin Teflon sheets are inserted between the loading plate and the rock for reducing friction. Additionally, 1 mm thick sheets of paper are placed between Teflon and loading plate for compensating remaining roughness of the specimen and, thus providing an almost constant pressure distribution. It follows the installation of the horizontal abutment for loading. The abutment consists of three massive steel rings put around the sample. The remaining slot between the inner surface of the rings and the loading plates is filled up with flat-jacks. These can be pressurized to up to 15 MPa. Vertical loading is realized by two further flat jacks, one above and one below the specimen. The vertical stresses may reach up to 30 MPa. The vertical abutment is completed by installing the fourth member and fixing the top steel plate with four nuts on the members. The strain on the abutment parts is continuously monitored as well as the displacement of the loading plates. Therefore, the stiffness of the abutment and the specimen can be derived from the loading cycle. Additionally, pressure in the two connected flat jacks of each loading direction is recorded continuously by pressure transducers. These indicate qualitatively initiation and growth of the hydraulically driven fracture. Pressure in the flat jacks was raised by hand pumps and shut in after the desired value had been reached. On initiation and opening of the fracture an increase of the pressure in the flat jacks was observed. This results from the fact that the specimen volume

increases with fracture volume. Currently we are modifying our loading device in such a way, that we can measure the volume changes during fracture growth by adjusting the pressure to a constant value.

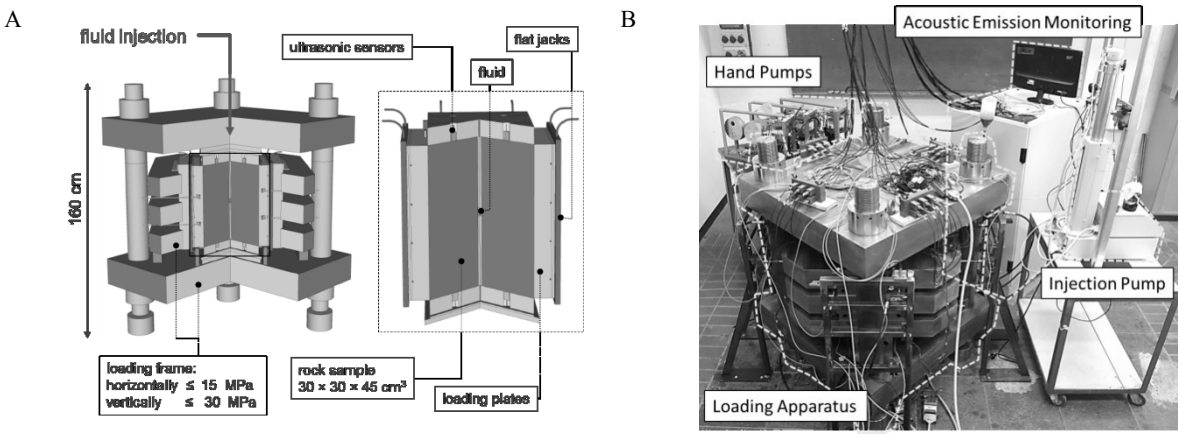

Figure 1: True-triaxial test facility; (A) Loading Apparatus; (B) Set-up in the lab.

The injection system includes a high-pressure injection pump, injection tubes, a packer which seals of the open-hole section and three pressure transducers. We use an Isco 260HP pump, which can inject in constant flow or constant pressure mode with a maximum pressure of 65 MPa and delivers information on the flow-rate, the remaining piston volume and the pressure at its head. The fluid is pumped to the packer through 1/8" steel tubes. For minimizing the air trapped in our system we can inject through the packer before starting the injection cycles. A ball-valve behind the packer is closed when we pressurize the open-hole section. Two pressure transducers are installed for monitoring the pressure in the borehole, one before and one behind the block at same distance to the packer. Before the injection procedure starts, the piston volume of the pump is reduced to a minimum. In this way the amount of stored energy at the point of fracture initiation is reduced, the total system stiffness increased and therefore better conditions for stable fracture growth are set. The minimum initial volume depends on rock permeability and strength, the compressibility of the fluid and the stress state.

For monitoring fracture propagation, 32 ultrasonic sensors are placed around the sample in a volume illuminating, irregular manner. For determining acoustic velocity, we run a series of active transmission experiments in which each sensor once acts as a transmitter while all others are recording. This is done right before and right after the fracturing experiment. The rock is already under confining pressure, the open borehole section is filled with fluid, but the fluid is not yet pressurized. During the fracturing experiments all sensors act as receivers recording the acoustic emissions. First arrivals are picked using Akaike's Information criterium [Maeda 1985] and events are localized using the optimum search algorithm of Nelder and Mead [Nelder and Mead 1965].

2.2 Status of the ongoing experiments

A variety of different issues can be studied with this new test facility. Our experiments put the focus on verifying a numerical code. In the corresponding fracturing experiments, we used specific injection procedures with different flow rates and fluids for ensuring slow fracture propagation. This is important for verifying the code since the volume of the rock sample is limited and the process of fluid-induced crack propagation is modeled numerically as a quasi-steady-state process. In section 2.2.4 we provide a brief overview regarding the experimental settings which will be employed in these experiments.

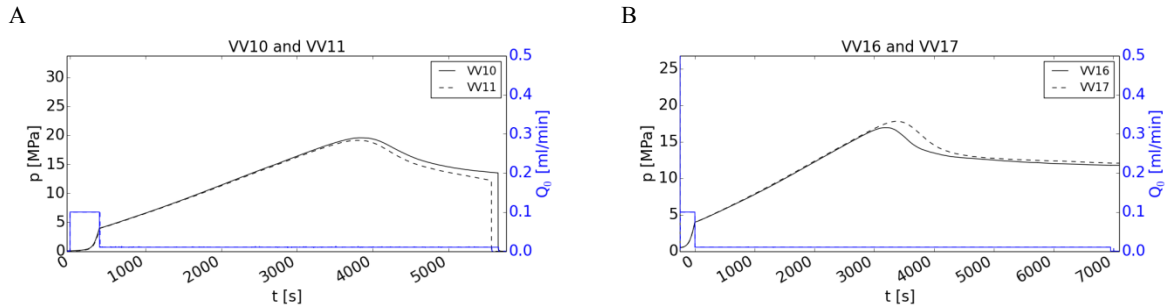

Figure 2: Reproducibility of the pressure curve for the second cycle of (A) "Black Belfast" Gabbro (Figure 3) and (B) "Titlinger Feinkorn" Granite (Figure 4).

2.2.1 Regime of verification

For ensuring a slow fracture propagation regime suitable for verification, we established a two-cycle injection procedure. During the first pressurization cycle we inject with a constant flow rate of 0.1 ml/min. Just right after breakdown, we stop injection and depressurize immediately (see Figure 3 and 4). This creates an initial fracture whose direction is determined by the confining stress

field and the initial notch carved into the open-hole section (see section 2.1). Then the fracture propagates in a second cycle with a slower flow rate of 0.01 ml/min. This second cycle will be the one used for verifying the XFEM fracture propagation code.

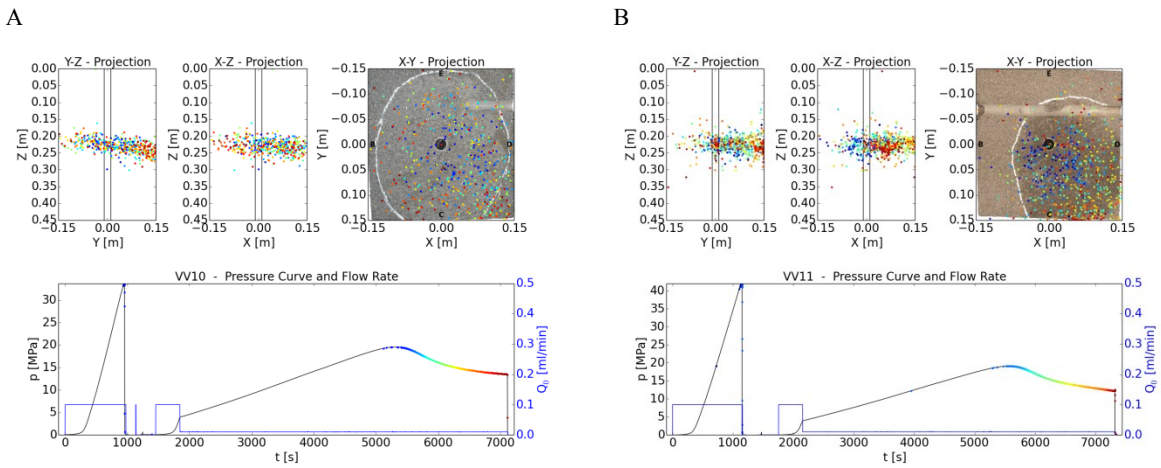

Figure 3: Repeated penny-shaped fracturing experiments performed on "Black Belfast" Gabbro under vertical confining pressure of 5 MPa and horizontal confining pressure of 15 MPa. Upper Row: X-Z-, Y-Z- and X-Y-projection of the sample. Acoustic emissions are represented by dots and colored according to time of occurrence. A picture of the sample opened up at the end is shown as background of the X-Y-projection. Lower row: Flow rate and fluid pressure curves. The two experiments have identical injection procedures, but differ in the vertical stress boundary condition: (A) electronically kept constant during fracturing (B) set at the beginning by closing valves, no adjustment during fracturing.

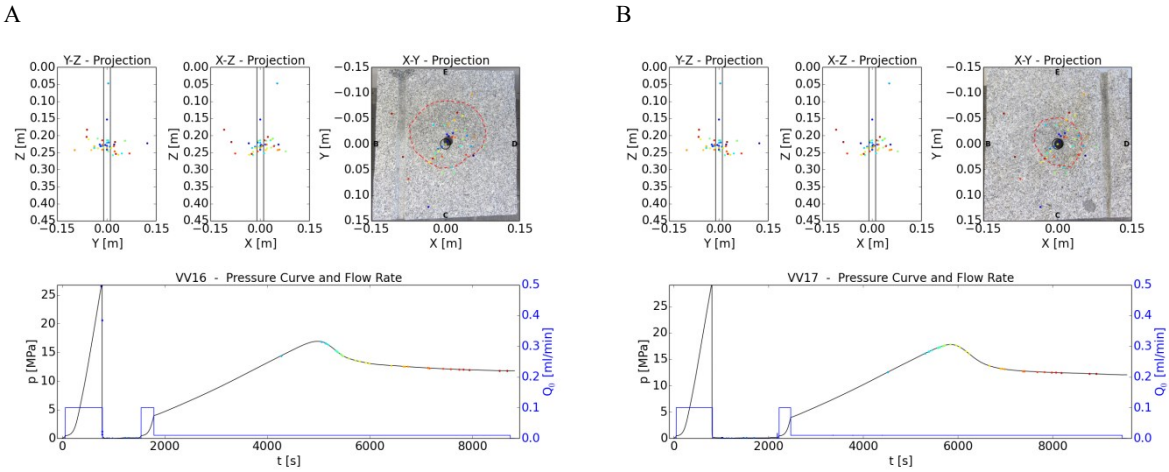

Figure 4: Repeated penny-shaped fracturing experiments performed on "Titlinger Feinkorn" Granite under vertical confining pressure of 5 MPa and horizontal confining pressure of 15 MPa. Upper Row: X-Z-, Y-Z- and X-Y-projection of the sample. Acoustic emissions are represented by dots and colored according to time of occurrence. A picture of the sample opened up at the end is shown as background of the X-Y-projection. Lower row: Flow rate and fluid pressure curves. The injection procedures were identical. The experiment here - in contrast to Figure 3 - terminated after the second cycle. The opened-up sample shows the fracture after the second cycle, which remained confined within the sample block.

2.2.2 Reproducibility

We repeat experiments at least once with identical injection procedure. As can be seen in Figure 2, experiments are quite reproducible for Gabbro and Granite with respect to the pressure curve. Dimension and shape of fractures are more variable (even for identical boundary conditions concerning vertical stress), but the orientation of the fracture within the stress field remains repeatable.

2.2.3 Slow fracture propagation

Since we simulate fluid-induced crack propagation numerically assuming a quasi-steady-state and since the maximum length of fracture is limited by the sample's dimension, slow and stable fracture propagation is required in the experiments for verification. In the "Titlinger Feinkorn" granite experiment (Figure 4), where we opened up the sample block right after the second cycle, the

penny-shaped fracture remained enclosed within the block. In the "Black Belfast" Gabbro experiment (Figure 3) additional injection cycles followed the second cycle before the opening-up of the sample block. We can't tell here from the final fracture surface how fast the fracture went in the second cycle, but the recorded acoustic emissions allow conclusions. The located acoustic events in the gabbro indicate (Figure 3) that the crack had already reached the sample's boundary after the second cycle. Therefore under nearly the same injection procedures, crack propagation was slower in "Titlinger Feinkorn" granite than in "Black Belfast" Gabbro. Currently we waiting for the results of the material parameter investigations (fracture toughness, Young's modulus, etc.) to proceed in interpretation.

The lower number of acoustic events recorded in "Titlinger Feinkorn" granite compared to the "Black Belfast" gabbro may be due to the different frequencies of the emissions in both cases: Generally lower in the granite than in the gabbro for which the frequencies fall into a band in which our sensors are particularly sensitive whereas they are close to the limits of sensitivity for the granite.

2.2.4 Verification procedures

For verifying the code we will : (1) compare experiments and simulation for penny-shaped cracks - a well-studied and still analytically tractable fracture scenario; (2) verify the relationship between fracture direction and state of stress by comparing changes in the stress regime with resulting changes in the fracture directions; (3) compare the results obtained for three different rock types: granite, basalt and gneiss; (4) use a higher-viscosity fracturing fluid for reaching different scaling regimes (viscosity dominated / toughness dominated) and testing the flow model assumptions. This last point raises questions on experimental issues which currently still need to be resolved.

3. FLUID INDUCED FRACTURE PROPAGATION SIMULATION

A number of physical processes are involved in a fluid-driven fracture: rock deformation due to fluid pressure on the crack faces, fluid flow within the fracture, and the fracture propagation. These physical processes are modeled separately in the XFEM fracture propagation code and solved by an iterative coupling. The strongly non-linear and non-local behavior makes fluid induced fracture modeling challenging. The extended finite element method (XFEM) is particularly suited for dealing with discontinuities. Unlike necessary mesh refinement around discontinuities required by the classical Finite Element Method, XFEM employs additional problem-specific functions (enrichments) added to the approximation space which account for these discontinuities.

3.1 Governing equations

The rock is considered as a homogenous, isotropic, linear-elastic solid. The material properties governing the deformation process are Young's modulus E, Poisson's ratio ν, and rock toughness KIC. The problem is described by the equations for the equilibrium of forces and the boundary conditions:

$$\nabla \cdot \boldsymbol{\sigma} + \boldsymbol{f} = 0 \text{ in } \boldsymbol{\Omega},\ \boldsymbol{u} = \boldsymbol{u}_0 \text{ on } \boldsymbol{\Gamma}_d,\ \boldsymbol{\sigma} \cdot \boldsymbol{n} = \hat{\boldsymbol{t}}_{\boldsymbol{n}} \text{ on } \boldsymbol{\Gamma}_n,\ \boldsymbol{p} \cdot \boldsymbol{n} = \hat{\boldsymbol{t}}_{\boldsymbol{I}} \text{ on } \boldsymbol{\Gamma}_I \qquad (1)$$

where $\boldsymbol{\sigma}$ is stress and $\boldsymbol{u}$ displacement defined on the domain $\boldsymbol{\Omega}$. In the following, we neglect body forces $\boldsymbol{f}$. Far-field stresses and fluid pressure **p** are imposed as Neumann boundary conditions on the outer boundary $\boldsymbol{\Gamma}_n$ and on the interface $\boldsymbol{\Gamma}_I$, respectively, where $\hat{t}_n$ and $\hat{t}_I$ denote traction. Fracture aperture *w* is obtained from the displacement field.

Based on Poiseuille's equation, flow of the fracturing fluid is modeled as laminar between two parallel plates. The model is valid for fractures with much larger crack length than width. As the fluid is further assumed to be incompressible and Newtonian the Reynolds (lubrication) equation for the flux is given by [Batchelor 1967]:

$$\frac{\partial w}{\partial t} - \boldsymbol{\nabla} \cdot \boldsymbol{q} + q_l = Q_0 \delta(\boldsymbol{x}) \quad , \quad \boldsymbol{q} = -\frac{w^3}{12\mu} \boldsymbol{\nabla} p \quad . \qquad (2)$$

The equation on the left describes the conservation of the fluid mass and is the local continuity equation. The one on the right defines the flux $\boldsymbol{q}$ with the dynamic viscosity μ, the crack opening width *w* and the pressure gradient $\boldsymbol{\nabla}$p. With the assumption of a fracture propagating into an impermeable solid, the leak-off term q_l is zero, and thus, can be neglected. A borehole is not considered in this study. As a consequence, the fluid flux is incorporated into the model as a point source (with the Dirac delta function $\delta(\cdot)$) at the center of the crack. Since the fluid is injected into the fracture at a constant rate Q_0 the volume of injected fluid is simply $V_f = Q_0 t$. The volume V of the created fracture equals the volume of injected fluid V_f and the amount lost to the surrounding rock-mass by the global volume balance condition:

$$V = \int_\Omega w \, \mathrm{d}\Omega = V_f - \int_0^t \int_\Omega q_l \, \mathrm{d}\Omega \, \mathrm{d}\tau. \qquad (3)$$

In the assumed quasi-static crack growth regime, the crack propagates continuously in a mobile equilibrium. In general, a number of various propagation criteria may be applied to this problem. These include local conditions based on stress intensity factors or the stress state in the vicinity of the crack front as well as conditions derived from global energy considerations. In terms of numerical implementation, only one node at the crack front is required to fulfill the critical condition $K_I = K_{IC}$, which states that the stress intensity factor K_I has to equal the fracture toughness K_{IC} of the material [Rice 1968]. Finally, the calculation of the propagation direction is based on the maximum circumferential stress criterion.

3.2 Numerical realization

XFEM is a method based on local partition of unity (PU, Melenk and Babuska 1996) which accounts for a priori knowledge on the solution characteristics by incorporating local enrichment functions into the finite element approximation space. This allows approximating accurately jumps, kinks, singularities, and other non-smooth features within elements [Belytschko and Black 1999,

Moes et al. 1999, Fries and Belytschko 2010]. In linear-elastic fracture mechanics, the standard XFEM formulation for the displacement approximation is:

$$\boldsymbol{u}^h(\boldsymbol{x}) = \underbrace{\sum_{i\in I} \boldsymbol{N}_i(\boldsymbol{x})\,\boldsymbol{u}_i}_{\text{continuous}} + \underbrace{\sum_{j\in I^{step}} \boldsymbol{N}^{\star}_j(\boldsymbol{x})\cdot\Psi_{step}(\boldsymbol{x})\,\boldsymbol{a}_j + \sum_{k\in I^{tip}} \boldsymbol{N}^{\star}_k(\boldsymbol{x})\cdot\left(\sum_{m=1}^{4}\Psi^m_{tip}(r,\theta)\,\boldsymbol{b}^m_k\right)}_{\text{discontinuous}} \qquad (4)$$

The classical FEM-approximation is described by the continuous part of the equation with continuous shape functions $\boldsymbol{N}_i(\boldsymbol{x})$ and nodal unknowns $\boldsymbol{u}_i$. Discontinuous characteristics across the crack path in the displacement field are accounted for by incorporating locally Step or Heaviside functions Ψ_{step} and additional nodal unknowns $\boldsymbol{a}_j$ at nodes within the set I^{step}. Nodes within I^{tip} are enriched with a set of four enrichment functions $\Psi^m_{tip}(r,\theta)$ which capture the singular behavior of the stress at the crack tip according to the linear elastic fracture mechanics (LEFM) theory. Additional degrees of freedom b^m_k are introduced locally into the approximation within the enriched region.

Due to the strong coupling of fluid and solid in hydraulic fracture problems, mainly confined to a small region near the crack tip [Detournay 1999], this problem is challenging to solve. The choice of the tip enrichment functions in XFEM traditionally is based on the inverse square-root singularity of Liner Elastic Fracture Mechanics (LEFM). Two limiting energy dissipation processes can by identified in case of a fluid-filled crack propagating into an impermeable rock,: the work done by the viscous fluid in expanding a fracture and the energy required to create new crack surfaces. In the toughness-dominated propagation regime, the dissipation energy for fracture creation is dominant and the effect of the crack tip process on the total fracture is described by the inverse square-root singularity of LEFM [Bunger et al. 2007]. Thus, the enrichment functions for classical fracture mechanic problems are also valid for this regime.

Two different crack descriptions are combined in this XFEM-approach, which proofed to be a major advantage in extending the XFEM formulation from 2D to 3D in a straightforward manner [Fries and Baydoun 2012]. On the one hand, an explicit crack description simplifies the crack update during the propagation. On the other hand, an implicit crack description obtained by means of the level-set method complements the XFEM extremely well and has become a standard in XFEM. The aim is to combine the advantages of each description, see [Fries and Baydoun 2012] for further details. Three level-set functions are defined which allow not determining the crack location also defininig a local coordinate system at the crack front (Figure 5):

- $\Phi_1(\mathbf{x})$ is the (un-signed) distance function to the crack path or crack surface. That is, the level-set value at position x is the shortest distance to the crack path or crack surface.
- $\Phi_2(\mathbf{x})$ is the (un-signed) distance function to the crack tip(s) or crack front. That is, the level-set value at position x is the shortest distance to the crack tip(s) or crack front.
- $\Phi_3(\mathbf{x})$ is a signed distance function to the crack path or crack surface which is extended over the whole domain. The sign is based on the direction of the normal vector of the segment that contains the nearest point.

(a) $\Phi_1(\mathbf{x})$ (b) $\Phi_2(\mathbf{x})$ (c) $\Phi_3(\mathbf{x})$

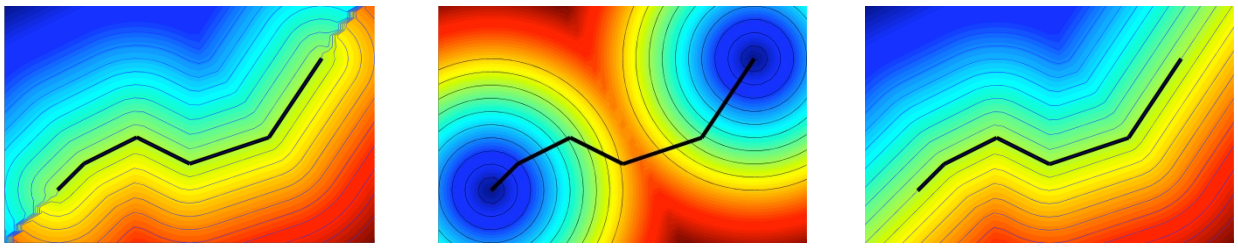

Figure 5: The level-set functions are illustrated for a 2D case [Fries and Baydoun 2012].

These level-set functions imply coordinate systems, which are used for defining the regions to be enriched and for evaluating the enrichment functions. Further, a coordinate system at the crack front is then used for determining the crack propagation direction and for adding new elements to the existing crack (Figure 6).

3.3 Simulation of a penny-shaped crack in a homogeneous 300 x 300 x 450 mm³ rock sample

We simulate crack propagation in a homogenous 300 × 300 × 450 mm^3 rock sample subjected to a horizontal load of 15 MPa and a vertical load of 5 MPa corresponding to the conditions in our laboratory experiment. Starting with an initial penny-shaped crack of 20 mm length the crack propagates continuously in the direction of the maximum stress in a quasi-static equilibrium. Only the crack growth is considered here while the crack initiation is not part of this study. The crack is filled with a Newtonian fluid of a dynamic viscosity of 1.48×10^{-6} [MPa s] at a constant injection rate of $Q_0 = 0.1$ ml/min.

Figure 7 shows the results of this simulation. The crack reaches the rim of the rock sample in approximately 1300 seconds and the total fluid volume pumped into the rock is around 2.17 ml. The pressure at the borehole decreases rapidly within the first 300

seconds and continues to decline slower to reach eventually a lower pressure limit of approximately 8 MPa. The crack opening (measured from the center of the crack), in contrast, increases until it flattens with time. However, numerical errors result from the relatively rough mesh of 27 × 27 × 27 elements used for discretizing the sample block.

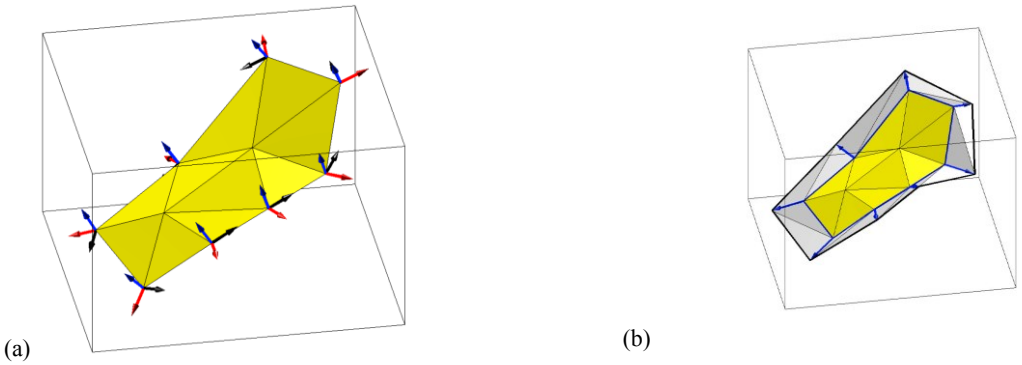

(a) (b)

Figure 6: (a) A coordinate system at the crack front. (b) New elements are added to the existing crack [Fries and Baydoun 2012].

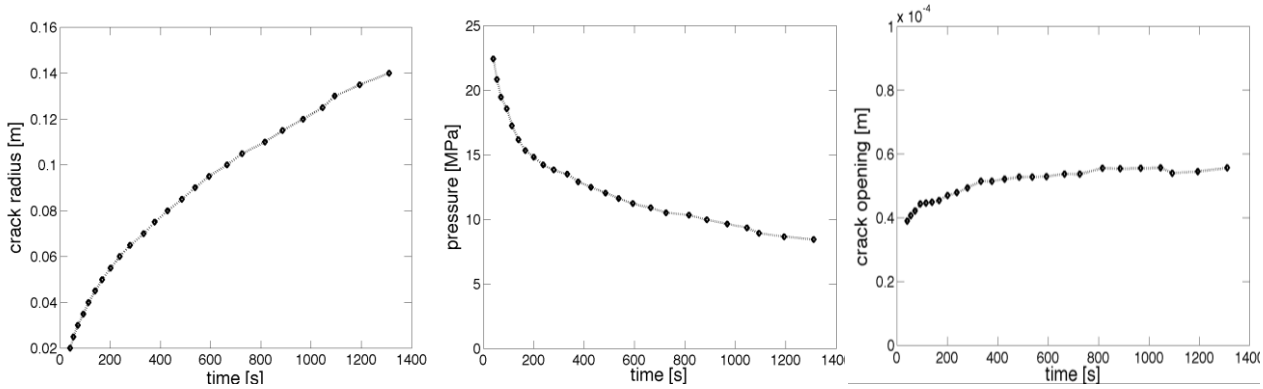

Figure 7: Simulation of a penny-shaped crack: Averaged radius of the penny shaped crack over time (left), fluid pressure at the borehole over time (middle) and fracture height at the borehole over time.

4. SUMMARY AND OUTLOOK

Laboratory experiments will allow us to verify an XFEM-code for simulating fracture propagation, to evaluate the validity of model assumptions, and to improve the XFEM-code and the experimental setup. The next step in code development will comprise an appropriate consideration of heterogeneities on fracture propagation and an extension to account for shear. Parallel to continuing experiments in the lab we will verify the code using small-scale field experiments.

REFERENCES

Batchelor G.: An Introduction to Fluid Dynamics. Cambridge University Press (1967).

Belytschko T., Black T.: Elastic crack growth in finite elements with minimal remeshing. *International Journal for Numerical Methods in Engineering* **45**, (1999), 601-620.

Brown D.W., Duchane D.V., Heiken G., Hriscu V.Th.: Mining the Earth's Heat: Hot Dry Rock Geothermal Energy. Springer (2012).

Bunger A., Detournay E., Garagash D., Peirce A.: Numerical simulation of hydraulic fracturing in the viscosity dominated regime. In SPE Hydraulic Fracturing Technology Conference, (2007).

Clauser C. (ed): Numerical simulation of reactive flow in hot aquifers. SHEMAT and processing SHEMAT. Heidelberg-Berlin: Springer (2003).

Detournay E.: Fluid and solid singularities at the tip of a fluid-driven fracture. In Durban D. and Pearson J.R.A. (eds), IUTAM Symposium on Non-linear Singularities in Deformation and Flow. Netherlands: Springer (1999), 27-42.

Fries T.-P., Baydoun M.: Crack propagation with the extended finite element method and a hybrid explicit–implicit crack description. *International Journal for Numerical Methods in Engineering* **89(12)**, (2012), 1527-1558.

Fries T.-P., Belytschko T.: The extended/generalized finite element method: An overview of the method and its applications. *International Journal for Numerical Methods in Engineering* **84(3)**, (2010), 253-304.

Gérard, A., Genter, A., Kohl, T., Lutz, P., Rose, P., Rummel,F.: The deep EGS (Enhanced Geothermal System) project at Soultz-sous-Forêts (Alsace, France), *Geothermics*, **35**, (2006), 473-483.

Maeda, N.: A method for reading and checking phase times in autoprocessing systems of seismic wave data. *Zisin=Jishin*, **38**, (1985), 365 – 379.

Melenk J. M., Babuska I.: The partition of unity finite element method: Basic theory and applications. *Computer Methods in Applied Mechanics and Engineering* **139(1-4)**, (1996), 289-314.

Moes N., Dolbow J., Belytschko T.: A finite element method for crack growth without remeshing. *International Journal for Numerical Methods in Engineering* **46,** (1999), 131-150.

Nelder, J.A., Mead, R.: A simplex method for function minimization. *Comput. J.*, **7(4)**, (1965), 308-313.

Rath V., Wolf A., Bücker M.: Joint three-dimensional inversion of coupled groundwater flow and heat transfer based on automatic differentiation: sensitivity calculation, verification and synthetic examples. *Geophysical Journal International* **167**, (2006), 453-66.

Rice J.: Mathematical analysis in the mechanics of fracture. In Liebowitz H. (ed), Fracture: An Advanced Treatise, Vol. 2 of Mathematical Fundamentals, Academic Press, New York, (1968), 191-311.